AN INEXPENSIVE DISTANCE MEASURING SYSTEM FOR NAVIGATION OF ROBOTIC VEHICLES

Cynthia Furse[1] and Nilesh Kamdar[2]
[1] Utah State University
Department of Electrical Engineering
Logan, Utah 48322-4120
[2] Agilent Technologies, Inc.

Received 22 October 2001

ABSTRACT: *Robotic vehicles operating indoors may be unable to receive the GPS signals that are commonly used for navigational control. This article describes an inexpensive system for location measurement in the absence of GPS with a range of 7.5 m and a resolution of 3 cm for a mass-produced cost of under $100.* © 2002 Wiley Periodicals, Inc. Microwave Opt Technol Lett 33: 84–87, 2002; Published online in Wiley InterScience (www.interscience.wiley.com). DOI 10.1002/mop.10241

Key words: *distance measurement; reflectometry*

INTRODUCTION

The use of data from the Global Positioning System (GPS), which provides accurate coordinate location information, has greatly simplified the navigational control of robotic vehicles. There are some applications, however, where GPS data are not available, such as inside shielded rooms, in gorges and deep mountain valleys, and more than a few feet inside many buildings. This distance-measuring system was developed for use in shielded rooms where microwave reflection off the metal or other dense walls is very high. The transmitter and receiver are located on the robotic vehicle, and measurements of the returned radar signals are used to accurately determine distance to all walls, thus giving a measure of the position of the vehicle within the room. Alternative configurations where the transmitter is located near the door to the room and the receiver is located on the vehicle could be substituted for applications (such as gorges or deep mountain valleys) where the reflections from the walls are poor or very cluttered. The system was developed for a range of 7.5 m and a resolution of 3 cm, and uses frequencies from 0.8 to 1.25 GHz in steps of 10 MHz. A larger frequency range and increased frequency resolution can be used to increase the range and/or resolution for other applications. The system could be mass produced for under $100.

This article describes the basics of the FDR system and how it was implemented. In addition, a variety of signal-processing techniques that are not traditionally used for FDR analysis are evaluated and compared to determine the best method for analyzing the data.

FREQUENCY-DOMAIN REFLECTOMETRY (FDR)

Frequency-domain reflectometry (FDR) was chosen for distance measurement because of its simplicity and low part count [1]. The FDR system is shown in Figure 1. The transmitted signal is swept in discrete steps over a given bandwidth. The signal is reflected back at the wall, and the reflected signal is compared with a copy of the transmitted signal with a balanced mixer used as a phase detector. The mixer is a square-law device, and outputs power directly proportionally to the squared magnitude of the received voltage, which is a standing wave produced by the sum of transmitted and received waves. The magnitude at the output of the mixer is given by

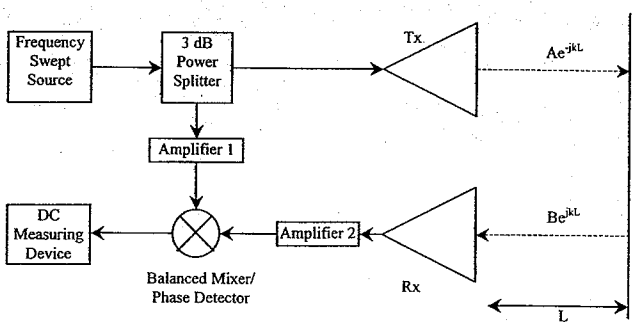

Figure 1 Frequency-domain reflectometer (FDR) system. The transmitted and received waves have wave number $k = 2\pi f/c$

$$|Ae^{-jkL} + Be^{jkL}|^2 = A + A\rho^2 + 2B\cos(2kL), \quad (1)$$

where the reflection coefficient $\rho = B/A$, the wave number $k = 2\pi f/c$, c is the speed of the wave, and the sweep frequency f is given in hertz. Equation (1) consists of a dc offset component $A + A\rho^2$, and a standing-wave component $2B\cos(2kL)$. The dc offset vanishes if a balanced mixer is used, as it is in this system. The standing wave pattern is then proportional to $\cos(2kL)$. For FDR measurements, the transmitted signal is swept in discrete steps over a range of frequencies $f_{BW} = f_2 - f_1$. Each stepped frequency gives a different phase change, each proportional to $\cos(2kL)$. Thus the output of the phase detector is a frequency-dependent dc voltage, caused by the bandwidth (f_{BW}) of stepped frequencies. This frequency-dependent dc voltage is a sinusoidal waveform [$\cos(2kL)$], with a dc offset ($A + A\rho^2$), and the number of cycles N in the bandwidth f_{BW} is proportional to the distance L, which is given by

$$L = \frac{cN}{2f_{BW}} \quad (2)$$

The range of the system, L_{max}, is limited by the Nyquist criterion. The source is swept between start frequency f_1 and stop frequency f_2 in discrete steps of Δf. The number of discrete frequencies is $N_F = f_{BW}/\Delta f$. This limits the number of samples that will be obtained in the dc voltage waveform $\cos(2kL)$ at the output of the mixer. The Nyquist criterion requires that the signal be sampled twice per cycle. As the distance being measured (L) increases, so does the number of cycles. At some point (the range L_{max}), there will not be enough stepped frequency samples to satisfy the Nyquist criterion and accurately compute L. The range is reached when only two frequency samples are taken per ($N = 1$) cycle of the dc voltage waveform:

$$L_{max} = \frac{c}{4\Delta f}. \quad (3)$$

A frequency resolution of 10 MHz will give a range of 7.5 m in air.

The resolution (accuracy) of the measurement is determined by the resolution of the Fourier transform that is used to find the number of cycles N in the dc voltage waveform. The number of points in the Fourier transform $N_{FFT} = 1/(\Delta f)(\Delta 2kL)$, so the resolution $\Delta L = c/(N_{FFT}\Delta f)$. The number of points in the Fourier transform, N_{FFT}, can be increased or decreased as desired to increase the resolution. This is done by zero-padding, adding zeros

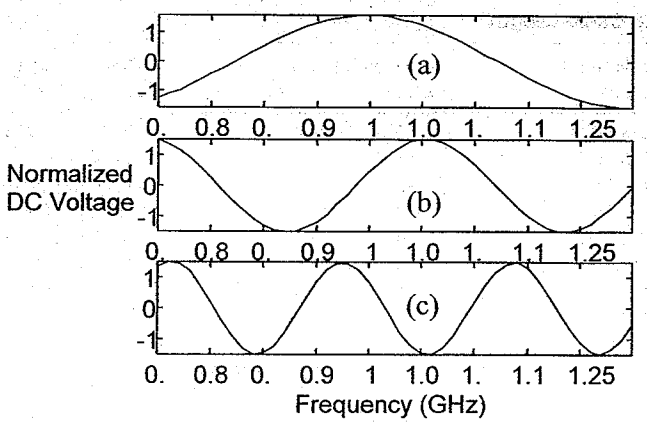

Figure 2 Simulated dc voltage waveforms. (a) $L = 40$ cm, (b) $L = 76$ cm, (c) $L = 122$ cm

in between the original sampled data. Additional measured samples are not needed, so the only limit to the number of samples that can be added is computational resources for computing the Fourier transform. For this system, $N_{FFT} = 1024$ that gives a resolution (expected error) of 2.9 cm for noise-free data.

Notably, both the range and resolution are independent of frequency. They depend only on velocity of propagation c, bandwidth f_{BW}, and frequency resolution Δf. A sweep of 0.8–1.25 GHz and a sweep of 8–8.45 GHz, each with 10-MHz resolution, would give the same range and resolution (this was, in fact, verified with the use of full circuit simulations). This gives a great deal of flexibility when one is choosing the circuit components. Components near 1 GHz were chosen for this application, because inexpensive electronics are available in this range, and the antennas needed for transmission and reception can be designed to be relatively small (less than 8 in. in maximum length).

SYSTEM SIMULATION

The complete system shown in Figure 1 was simulated with the use of HP/EEsof Libra software, Series IV. To facilitate testing and debugging, the transmit and receive antennas and distance L to the wall were initially replaced with a single cable of length L (having a typical velocity of propagation of 2×10^8 m/s). This eliminated transmission losses, spurious reflections, antenna mismatches, et cetera, when the circuit was built and tested. Figure 2 shows the dc voltage waveforms over the frequency range 0.8–1.25 GHz for three different lengths of cables. As expected, the longer cables have more cycles. The data from these dc voltage waveforms was used to predict the lengths of the cables with the use of the Fourier transform with different lengths N_{FFT}. The results from this prediction are shown in Table 1 along with the expected errors [$\Delta L = c/(N_{FFT}\Delta f)$] and the observed errors. This demonstrates the effectiveness of the method on noise-free data. Additional error is expected with real data.

SYSTEM IMPLEMENTATION

The system was built with the use of standard commercial components. The *frequency-swept source* was a voltage-controlled oscillator ZOS-1025 from Mini-Circuits [2]. A Mini-Circuits ZFSC-2-11 3-dB power splitter was used to divide the power equally so that half the power is transmitted while the other half is used as a comparison for the received wave. The Mini-Circuits ZLW-2 balanced mixer is used as a phase detector. The Mini-Circuits ZFL-1000LN low-noise amplifier was used to amplify the received signal. An 8-bit A/D converter was used to read the dc

TABLE 1 Predicted Cable Lengths with the Use of Different-Sized Fourier Transforms. Values Shown Include Expected and Observed Errors for Three Different Cable Lengths. The Simulated dc Voltage Waveforms from which these Data are Derived are Shown in Figures 1(b) and 1(c) for the 76- and 122-cm Cables, Respectively

N_{FFT}	46	512	1024	2048
Expected error (cm)	(43.)	(3.9)	(1.9)	(1.0)
Actual L (cm)	Predicted L (cm) (Observed Error)			
75.692	44.44 (31.25)	70.45 (5.24)	74.29 (1.40)	75.23 (0.46)
122.7	88.88 (33.8)	117.42 (5.28)	121.21 (1.49)	121.153 (1.55)
182.88	133.33 (49.55)	180.04 (2.84)	181.82 (1.06)	182.71 (0.17)

voltage output from the mixer into a computer, which was used for processing of the data. Later versions of this system use an SIC microcontroller from Management Sciences, Inc. to replace the personal computer.

The dc voltage waveforms and associated distance computations for various cables are shown in Figure 3. These correspond to the simulated waveforms shown in Figure 2 for the same lengths of cables. The two sets of waveforms are very similar, except that the experimental waveforms are inverted. This is because the mixer is an inverting mixer, and it has no effect on computation of line length.

COMPARISON OF SIGNAL PROCESSING METHODS

The resolution of the Fourier transform clearly controls the accuracy of the data [$\Delta L = c/(N_{FFT}\Delta f)$]. This or other signal-processing techniques are used to determine the number of cycles in the dc voltage waveforms such as those shown in Figures 2 and 3. The traditional method of analyzing FDR data is to use a Fourier transform. The standard Fourier transform with zero padding on the end of the test points was compared to other methods, including the Fourier transform with additional interpolated data or interspersed zero points, a mathematical modeling method, and a simple location of the zero crossings of the waveforms.

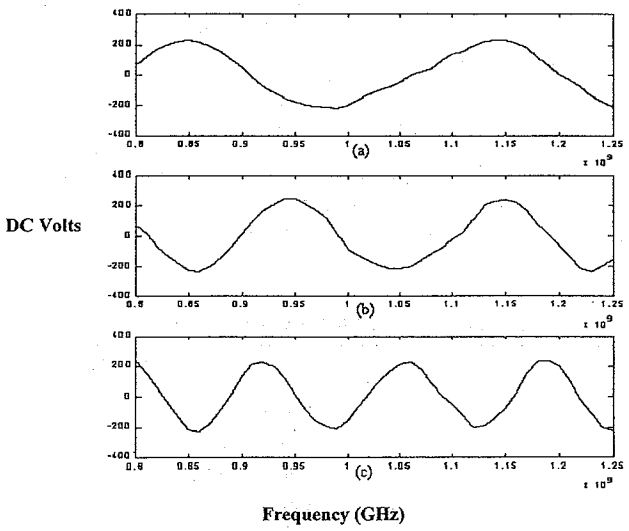

Figure 3 Experimentally observed dc voltage waveforms. Compare to simulated waveforms in Figure 2. Experimental results are inverted because of the use of an inverting mixer. (a) $L = 40$ cm, (b) $L = 76$ cm, (c) $L = 122$ cm

TABLE 2 Comparison of Signal Processing Methods for Determining Cable Length

Actual (cm)	Fourier Transform w/Zero Padding at End (cm) (% Error)	Math. Model (cm) (% Error)	FFT with Linear Interp. (cm) (% Error)	Zero Crossing (cm) (% Error)
40	49.83 (19.73%)	56.06 (28.65%)	50.8 (21.26%)	44.46 (10.03%)
61.59	68.39 (9.94%)	73.36 (16.04%)	66.44 (7.3%)	64.36 (4.3%)
75.69	81.09 (6.66%)	90.1 (16%)	82.07 (7.77%)	80.386 (5.84%)
122.7	129.94 (5.58%)	135.45 (9.41%)	128.97 (4.86%)	131.72 (6.85%)
182.88	193.45 (5.47%)	197.22 (7.27%)	191.5 (4.5%)	194.57 (6%)
250.82	264.77 (5.27%)	265.8 (5.64%)	265.75 (5.62%)	270.124 (7.14%)
441.96	454.32 (2.72%)	454.68 (2.8%)	453.35 (2.51%)	457.46 (3.39%)
Max % error	9.94%	16.04%	7.77%	7.14%
Max error (cm)	13.95	14.98	14.93	19.3

The standard Fourier-transform method with zero padding simply adds additional zeros on the end of the signal to increase the length and hence the resolution of the Fourier transform. This method adds a high-frequency step at the end of the data that adds a small amount of error to the calculation. Ideally, additional measurements (addition stepped frequencies) would have been used, but this would have prohibitively increased the cost and complexity of the system. Alternative methods of increasing the number of data points (and hence the resolution) for the Fourier transform are to interpolate between the measurements with the use of either a linear or cubic interpolation or to add zeros in between each measured data point.

Another method [3] of computing the number of cycles in the dc voltage waveforms is to model the sinusoid as a linear mathematical function

$$x(n) + a_1 x(n-1) + a_2 x(n-2) = 0. \tag{4}$$

There are many data points $x(n)$, and two unknowns a_1 and a_2. This can be written as a matrix equation

$$\begin{bmatrix} x(2) & x(1) \\ x(3) & x(2) \\ x(4) & x(3) \\ \cdots & \cdots \end{bmatrix} \begin{bmatrix} a_1 \\ a_2 \end{bmatrix} = - \begin{bmatrix} x(0) \\ x(1) \\ x(2) \\ \cdots \end{bmatrix}. \tag{5}$$

The values of a_1 and a_2 are obtained from (5) and substituted into (4), which is then solved for $x(n)$. The solution of (4) has the characteristic form

$$z^2 + a_1 z + a_2 = 0. \tag{6}$$

The roots of (6) are complex conjugates, and because the data are sinusoidal, they lie on a circle with unit magnitude. The angle of any one of the roots is the frequency relative to the sampling frequency, which has an angle of 360°. The drawback of this method is that it is quite sensitive to noise.

The zero-crossing method finds the locations where the waveform crosses zero by finding a point above and a point below zero and linearly interpolating between them. Table 2 gives a comparison of these different signal-processing methods for experimental data on several different cable lengths. The zero-crossing method was best for short lengths of cable, and the Fourier-transform method was best for longer lengths. Fourier transformation with linear interpolation was better than either the Fourier transform with zero padding on the end or in between the measured points. The mathematical modeling method was found to be best with noise-free simulated data, but the noise in the data reduced its accuracy for the measured results.

TESTS WITH ANTENNAS

Two types of antennas were used for testing the final performance of this system—a half-wave dipole antenna and a commercial log-periodic antenna (LPA) (Model NA-4000-2G from Tempest, Inc.). The dipole antennas are omnidirectional, and the LPA antennas are highly directional. Both antennas were well matched to the system to minimize reflections within the system. No effort was made to prevent a direct path from the transmitting to the receiving antenna. Ideally one would want a directional antenna (such as an LPA) to be used as both the sending and receiving antenna, so that the distance to each wall could be determined separately. A dipole antenna was also examined for its use as a receiving antenna, because it is simple and can be mounted on a robotic vehicle for other communication applications. The distance to a metal wall in a shielded room was measured with the use of LPA-LPA and LPA-dipole antennas. Table 3 gives the experimental predictions of cable length from the completed system. Both systems performed adequately, so it can be assumed that this method can be used for robotic navigation.

TABLE 3 Distance to the Wall Measured with the Use of LPA-LPA Antennas and LPA-Dipole Antennas in a Metal Screen Room

	LPA–LPA Antennas		LPA–Dipole Antennas	
Actual Length (cm)	FFT (cm) (% Error)	Math. Model (cm) (% Error)	FFT (cm) (% Error)	Math. Model (% Error)
38	44 (13.64%)	46.3 (17.93%)		
64	68.8 (6.98%)	64.1 (0.16%)	67.88 (6.06%)	64.64 (1.0%)
98	109.2 (10.26%)	100 (2%)	96.32 (1.71%)	95.3 (2.75%)
124	145.1 (14.54%)	133 (6.77%)		
154	172.9 (10.93%)	165.3 (6.84%)		
184	197.56 (6.86%)	185.3 (0.7%)		
Max % error	14.54%	17.93%		
Max absolute error (cm)	21.1	11.3		

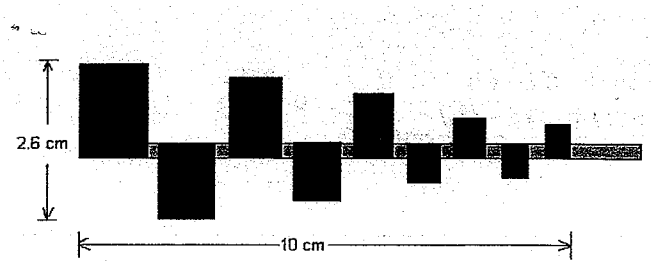

Figure 4 Microstrip log-periodic antenna

Because the log-periodic antennas provided the most stable results, a set of microstrip log-periodic antennas were built with the dimensions shown in Figure 4 following the methods described in [4]. Microstrip antennas are highly desirable for this application, because they are inexpensive and rugged and can be mounted flush on the top (roof) of the robotic vehicle.

CONCLUSIONS

A swept frequency reflectometer system was built for determining distance to metal walls for a robotic navigation system. Several different signal-processing methods were compared, and it was found that the simple Fourier-transform provided the best overall results, although each of the methods tested had applications where it was optimal. Log-periodic antennas were generally found to provide the most stable results.

REFERENCES

1. D.A. Noon, A computer controlled microwave distance measuring system, B.E. thesis, University of Queensland, Australia, 1991.
2. RF/IF Designer's Guide—Mini-Circuits, DG-98/99, Mini-Circuits, New York, 1998.
3. T.K. Moon and W.C. Sterling, Mathematical methods and algorithms, Prentice Hall, Englewood Cliffs, NJ, 1999, pp. 396–397.
4. J. Huang, Microstrip Yagi array antenna for mobile satellite vehicle application, IEEE Trans Antennas Propagat AP-39 (1991), 1024–1030.

SINGULAR BEHAVIOR OF THE BERENGER AND LEAKY-MODES SERIES COMPOSING THE 2D GREEN'S FUNCTION FOR THE MICROSTRIP SUBSTRATE

Hendrik Rogier and Daniël De Zutter
Information Technology Department
Ghent University
St. Pietersnieuwstraat 41
Ghent, Belgium

Received 25 October 2001

ABSTRACT: *The singular behavior of the modal expansions is examined in Berenger and leaky modes for the Green's functions G_A and G_V of a 2D microstrip substrate. When the excitation point approaches the source point, and both are lying in the microstrip substrate, the Green's function exhibits a singularity that corresponds to the open configuration without a perfectly matched layer. This observation remains valid when one or both points are lying on the substrate–air interface, unless G_A is being considered for a nonmagnetic ($\mu_r = 1$) substrate. In the latter case a different singularity is obtained when both excitation point and source point are lying on the interface. That singularity is of a higher order and depends on the characteristics of the PML.* © 2002 Wiley Periodicals, Inc. Microwave Opt Technol Lett 33: 87–93, 2002; Published online in Wiley InterScience (www.interscience.wiley.com). DOI 10.1002/mop.10244

Key words: *integral equation techniques; Green's functions for multilayered media; perfectly matched layers*

1. INTRODUCTION

The efficient and accurate calculation of the Green's functions for multilayered media still remains an important research topic. In [1, 2], a new technique was proposed to evaluate the Green's function of a microstrip substrate by using perfectly matched layers (PMLs) [3–5] in an analytical way. When the open microstrip substrate is terminated by means of a PML, an efficient problem description in terms of a set of discrete modes of the closed waveguide containing the PML is possible, while the PML efficiently mimics an open structure. Some recent publications, have classified the modes supported by these waveguides into leaky and Berenger modes [6], and the series of leaky and Berenger modes have been analyzed when the source point approaches the excitation point [7]. This is an important issue, because both modal series converge exponentially when source and excitation point are well separated, but convergence tends to get lost at closer distances. This is not surprising, because the Green's functions should exhibit singular behavior when the source point approaches the excitation point.

This Letter will show that, when the excitation point approaches the source point, and both are lying in the microstrip substrate, the modal series composing the Green's function G_A and G_V of a 2D microstrip substrate exhibit the correct singular behavior related to the open structure. In some cases, it will be seen that each separate series of Berenger or leaky modes exhibits a higher-order singularity than the one expected for the open structure. However, it will be shown that the singularities of the Berenger and leaky mode parts compensate to yield the correct singularity. This is of importance for the efficient numerical evaluation of the modal expansions in a field simulator. When G_A is analyzed in Section III, both magnetic ($\mu_r \neq 1$) and nonmagnetic ($\mu_r = 1$) substrates are considered. For the latter, a distinction is made between the situation in which the excitation is lying inside the substrate and not on the interface and the case in which both excitation and observation points are lying on the interface. In that case, the singularity does not correspond to the one obtained in an open structure, but it is of a higher order and depends on the characteristics of the PML. When G_V is considered in Section IV, the substrate is assumed to be dielectric ($\varepsilon_r \neq 1$). In Section V, the theoretical results are illustrated on a sample configuration.

2. MODAL EXPANSIONS FOR G_A AND G_V

Consider a microstrip substrate with permittivity ε_r, permeability μ_r, and thickness d. By terminating the air region with a perfectly matched layer (PML), as shown in Figure 1, a modal expansion in leaky modes and Berenger modes [6] can be found that approximates the Green's functions G_A and G_V for the open microstrip configuration. Specifically, in [7] it is shown that for a source lying in or on top of the microstrip substrate ($0 < z' \leq d$), the Green's function in or on top of the substrate ($0 < z \leq d$) can be written as